



**HAL**  
open science

# A non-collinear fretting-fatigue experiment to compare multiaxial fatigue criteria: critical shear plane strategy is better than invariant formulations

Camille Gandiolle, Simon Garcin, Siegfried Fouvry

## ► To cite this version:

Camille Gandiolle, Simon Garcin, Siegfried Fouvry. A non-collinear fretting-fatigue experiment to compare multiaxial fatigue criteria: critical shear plane strategy is better than invariant formulations. Tribology International, 2017, 108, pp.57-68. 10.1016/j.triboint.2016.09.011 . hal-01526045

**HAL Id: hal-01526045**

**<https://hal.science/hal-01526045>**

Submitted on 19 Oct 2023

**HAL** is a multi-disciplinary open access archive for the deposit and dissemination of scientific research documents, whether they are published or not. The documents may come from teaching and research institutions in France or abroad, or from public or private research centers.

L'archive ouverte pluridisciplinaire **HAL**, est destinée au dépôt et à la diffusion de documents scientifiques de niveau recherche, publiés ou non, émanant des établissements d'enseignement et de recherche français ou étrangers, des laboratoires publics ou privés.

# Development of non collinear fretting fatigue experiment to compare multiaxial fatigue criteria: critical shear plane strategy better than invariant formulations

---

C. Gandiolle<sup>1\*</sup>, S. Garcin<sup>1</sup>, S. Fouvry<sup>1\*</sup>

<sup>1</sup> LTDS, Ecole Centrale de Lyon, 36 avenue Guy de Collongue, 69134 Ecully, France

\* corresponding authors

E-mail addresses: [camille.gandiolle@ec-lyon.fr](mailto:camille.gandiolle@ec-lyon.fr), [Siegfried.fouvry@ec-lyon.fr](mailto:Siegfried.fouvry@ec-lyon.fr)

## Abstract

Fretting fatigue crack nucleation is usually predicted with multiaxial fatigue criteria combined with a non-local approach to take account of the severe fretting stress gradient. Conventional collinear fretting fatigue loadings, being quasi-uniaxial near the hot spot surface contact border, lead to similar predictive results whatever the non-local approach and fatigue criterion. To differentiate between approaches, a new non collinear fretting fatigue set up allowing applying fatigue stress with a  $\beta$ -angle versus the 'x' fretting direction was developed. Using this new test device, the crack nucleation condition of 35NiCrMo16 low alloyed steel was investigated for a sphere/plane configuration as a function of the  $\beta$  misalignment angle. These results were compared to usual plain fretting and collinear fretting fatigue results. Then using representative 3D elastic simulations, it was possible for the first time to discriminate the performance between critical plane SWT and McDiarmid versus Crossland and Dang Van invariant formulations. Experiments and modelling suggested that McDiarmid criterion provides the best crack nucleation predictions.

Keywords: Fretting-Fatigue; non-collinearity; multiaxial; crack nucleation; multiaxial fatigue criteria

## Highlights

- Development of innovative non-collinear fretting fatigue test-device
- Real multiaxial fretting fatigue crack nucleation analysis
- Calibration of length scales for non-local analysis from plain fretting experiments
- Best prediction of cracking risk considering McDiarmid criterion with maximum shear critical plane
- Crack nucleation location allow easy quantification of fatigue stress influence regarding fretting loading

## 1. Introduction

Fretting is defined as a small oscillatory movement between two bodies in contact. Combined with cyclic bulk fatigue loading, so-called fretting-fatigue loading can induce catastrophic damage such as wear or cracking, which critically reduces the endurance of assemblies [1]. It is essential for industries to be able to prevent such failure.

Fretting involves two sliding conditions depending on the displacement amplitude: partial slip, which involves an inner stick zone, and larger amplitude gross slip, inducing a full sliding response in the interface. Partial slip condition, which induces cyclic stressing but nearly no friction dissipation leads

primarily to cracking damages. Gross slip condition which promotes high friction dissipation, favors surface wear which softens pressure and shear distributions, and tends to reduce the cracking phenomenon [2–4].

In this investigation we focus on crack nucleation under partial slip. Fretting fatigue crack nucleation was extensively investigated during the past two decades. To capture the very complex stress state imposed by contact loading, multiaxial fatigue criteria like Dang Van or SWT approaches were considered [5–7]. These approaches allowed predicting the crack nucleation location which was systematically observed on surface at the contact border. However quantitative analysis showed some discrepancy with experimental results. The fatigue stress analyses which were performed at the hot spot stress of the contact interface led to conservative crack nucleation predictions. Indeed fretting stressing is characterized by very severe stress gradient conditions so that non local fatigue stress analysis are required.

Transposing research works developed on notch fatigue problem [8,9], a first approach consisting in averaging the stress state over a representative “process volume” of cubic length  $l_v$  was introduced. Transposed to multiaxial frame work, this non local multiaxial strategy was shown to well predict plain fretting cracking (i.e. without external bulk stress), fretting on pre-stressed fatigue specimen and usual fretting fatigue conditions [10,11]. Successful results were also obtained considering an equivalent critical distance approach instead of an averaging volume. The stress state in this case was defined at a,  $l_D$ , critical distance below the hot spot [12]. Further investigations demonstrated that process volume and critical distance are nearly equivalent. Indeed the mean stress state of a cubic volume is nearly equivalent to the stress state imposed at the center of this latter which infer that  $l_D \approx l_v/2$  [13].

A key aspect of these approaches is the determination of pertinent  $l_v$  and  $l_D$  intrinsic length values. Extending Taylor’s development [14], Araujo and co-authors suggested that the optimal critical distance can be related to the half value of the crack length defining the transition from short to long crack propagation regime  $l_D = b_{\phi}/2$  [12], which can be extrapolated from  $\Delta K_{\phi}$  and  $\sigma_d$  fatigue data using Kitagawa description [15].

More recently, Gandiolle et Fouvry by introducing a  $b_{opt} - l_{opt}$  concept suggested that Taylor’s approach was reliable according that the crack length used to define the crack nucleation condition is equal to the short to long crack propagation transition (i.e.  $b_{CN} = b_{\phi}$ ) [16]. For smaller crack flaw analysis (i.e.  $b_{CN} < b_{\phi}$ ) the Taylor’s approach is no more consistent and alternative strategies which consists in calibrating the optimal  $l_D$  and  $l_v$  length scales from reverse analysis of plain fretting crack results appears more pertinent ( $l_{D(PF)}$  or  $l_{V(PF)}$ ). Using this strategy the very severe stress gradient imposed by contact loadings was better considered and conservative fretting fatigue crack predictions are achieved.

A major conclusion extracted from these research works was that whatever the fatigue stress formulation, very good predictions are achieved if the non-local length scales parameters were properly identified. It must be underlined that all the fretting fatigue experiments used to calibrate such approaches were collinear (i.e. the fatigue stress was the same direction as the fretting sliding) leading to a quasi-uniaxial stress along the ‘x’ direction near the hot spot surface contact border. This can explain why it was not possible to differentiate between multiaxial fatigue criteria.

To palliate such limitations, a new non collinear fretting fatigue set up allowing applying fatigue stress with a  $\beta$ -angle versus the ‘x’ fretting direction was developed. Using this new test device, a 35NiCrMo16 low alloyed steel was investigated, defining the threshold crack nucleation condition

( $b_{CN}=10\mu\text{m}$ ) at  $10^6$  cycles for a sphere/plane configuration as a function of the  $\beta$  misalignment angle. These results were compared to usual plain fretting and collinear fretting fatigue results. The stress gradient effect was calibrated by defining critical distance ( $l_D$ ), process volume ( $l_V$ ) but also line averaging ( $l_L$ ) length scale from plain fretting crack nucleation results. Finally by combining all these experimental results with representative 3D elastic simulations, it was possible for the first time to discriminate the performance between multiaxial fatigue criteria based on critical plane approach (SWT and McDiarmid) or invariant formulations (Crossland and Dang Van).

## 2. Experimental approach

### 2.1. Materials

The studied material is a 35NiCrMo16 low-alloyed steel displaying a tempered martensitic structure. The fatigue and fracture properties of this alloy and equivalent structures were extensively investigated by Galtier, Henaff and Fouvry [17–19]. The mechanical and fatigue properties are listed in Table 1. Chromium 52100 steel was chosen for the spherical counter bodies in order to maintain elastically similar conditions whilst simultaneously ensuring that cracks arose only in fatigue 35NiCrMo16 specimens. Both plane and spherical pad surfaces were polished to achieve a controlled surface roughness of  $R_a=0.4\mu\text{m}$ .

Table 1. Mechanical and fatigue properties of studied steels

Material	E (MPa)	$\nu$	$\sigma_{y,0.2\%}$ (MPa)	$\sigma_U$ (MPa)	$\sigma_d$ (MPa)	$\tau_d$ (MPa)
35NiCrMo16	205000	0.3	810	1130	575	386
52100	195000	0.3	1500	-	-	-

E: Young's modulus;  $\nu$ : Poisson's coefficient;  $\sigma_{y,0.2\%}$ : Yield stress (0.2%);  $\sigma_U$ : ultimate stress;  $\sigma_d$ : traction-compression fatigue limite ( $R_\sigma=\sigma_{\min}/\sigma_{\max}=-1$ ;  $10^7$ cycles);  $\tau_d$ =shear fatigue limite ( $R_\tau=-1$ ;  $10^7$ cycles).

### 2.2. Contact

A single sphere on plane contact was investigated (Fig. 1). 52100 pads were machined to achieved a  $R=200\text{mm}$  spherical radius. All tests were performed for a constant normal force,  $P=5000\text{N}$  inducing a maximum Hertzian contact pressure,  $p_{\max}=663\text{MPa}$ , and a Hertzian contact radius,  $a_H=1.90\text{mm}$ . Tests were systematically performed under partial slip conditions. Under these conditions, cracking is the main damage mechanism as wear of the contacting surfaces is small, and the friction coefficient  $\mu$  is roughly constant during test. In all cases, the Von Mises criterion of yielding indicates than no macroscopic plastic yield occurs.

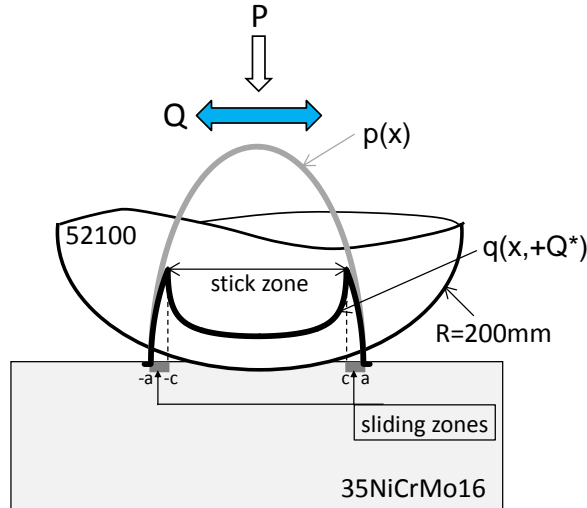


Figure 1: sketch of sphere on plane contact with partial slip; surface pressure profile  $p(x)$  (—) and surface shear profile  $q(x)$  (---).

### 2.3. Experimental test conditions

All the experiments used in this investigation are instrumented to achieve an online control and recording of normal force,  $P$ , fretting displacement  $\delta(t)$ , tangential force  $Q(t)$  and potentially fatigue stress  $\sigma(t)$  for fretting fatigue configuration. We focus on high fatigue crack nucleation so tests were systematically performed up to  $10^6$  loading cycles at 12Hz. Three test configurations have been considered (Fig. 2): plain fretting, conventional collinear fretting fatigue and non collinear fretting fatigue.

#### 2.3.1. Plain fretting test

A first set of experiment were performed using a so-called plain fretting configuration (PF). A static normal force was applied by a mechanical trolley whereas alternated cyclic displacement amplitude  $\delta^*$  was imposed using a single hydraulic actuator to achieve a constant partial slip tangential force amplitude  $Q^*$  [10]. A major interest of this test is to investigate the fretting cracking process by only considering the contact loading. Because of the alternated tangential loading and because no bulk stress is imposed, the sliding zones and related shear profile remains symmetrical like described by Mindlin's formalism [20].

#### 2.3.2. Collinear fretting fatigue test

A second set of experiments was performed using a conventional collinear double actuator fretting fatigue test (FF) that allows separate application of fretting and fatigue loadings (Fig. 2). This test was inspired from the experimental set-up developed by Hills and coworkers [21]. Full details of the experiment used in this investigation can be found in [22]. Both tangential force amplitude  $Q^*$  and fatigue stress  $\sigma_f$  were applied in phase so that the maximum fretting load  $+Q^*$  was applied at the same time as the maximum fatigue stress  $\sigma_{F,max}$ .

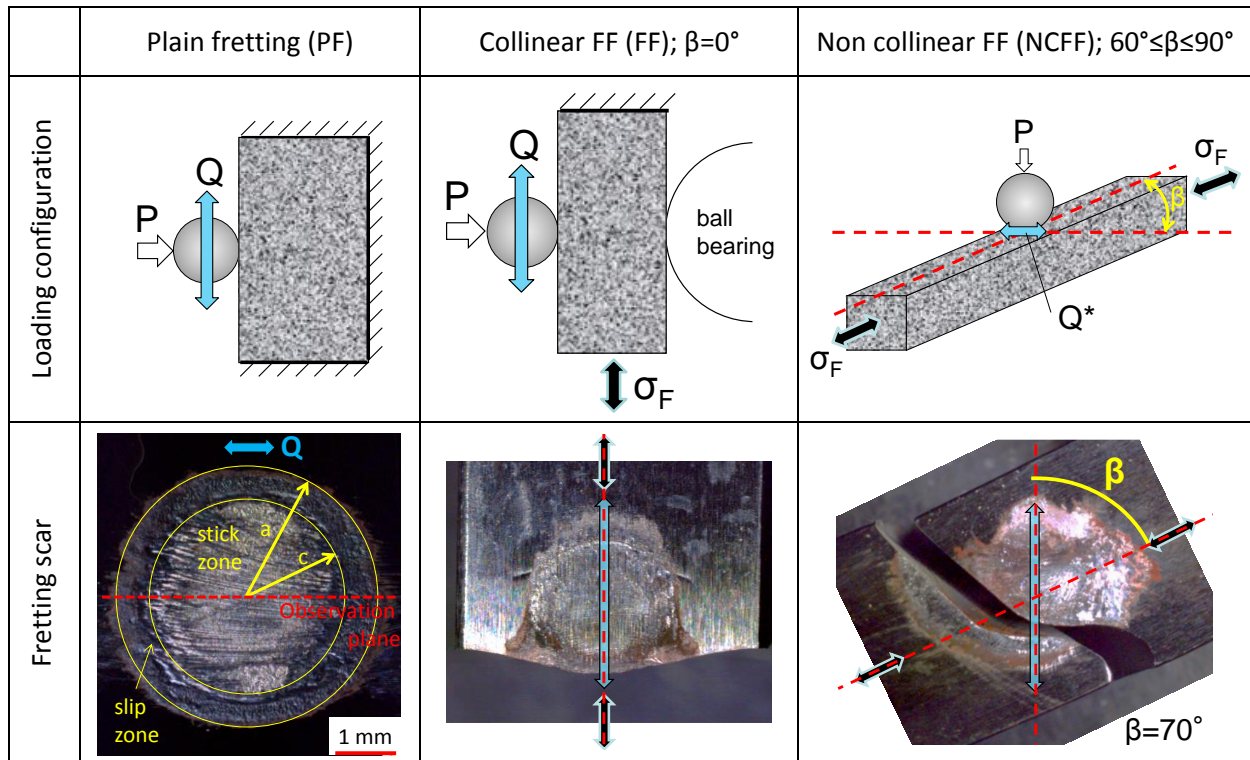


Figure 2: Loading configurations and related fretting scars for the three test configurations: plain fretting, conventional collinear fretting fatigue and on collinear fretting fatigue. ( $R=200\text{mm}$ ,  $P=5000\text{N}$ ,  $Q^*=2700\text{N}$ ,  $\sigma_{F,\text{max}}=400\text{MPa}$ ,  $R_\sigma=0.8$ ,  $10^6$  cycles).  $\longleftrightarrow$ : Fretting loading direction;  $\blackleftarrow\blackrightarrow$ : fatigue loading direction.

### 2.3.3. Non collinear fretting fatigue test

A third set of non collinear fretting fatigue tests (NCF) were performed using a new triple actuator device developed in the LTDS (Fig. 2). In this innovative test set-up, fatigue sample was maintained between two fatigue actuator so that the central point of the sample remained fixed (centroid fatigue stress condition). The fretting loading was applied through the third actuator on this central point. The fretting apparatus was installed on a moving platform which allowed varying the angle between the fretting and fatigue loadings in a range between  $\beta=60^\circ$  and  $\beta=90^\circ$ .

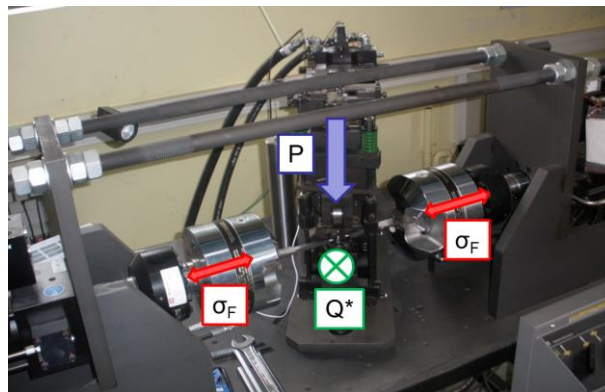


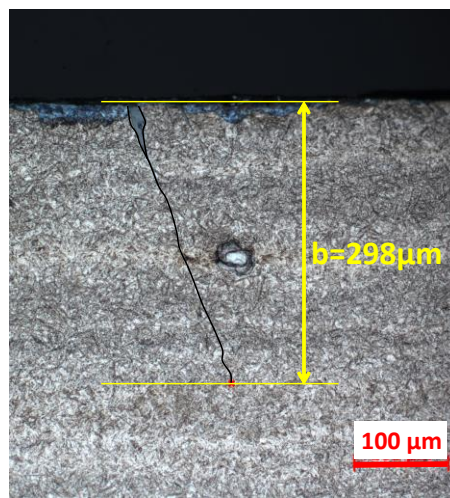
Figure 3: Multi-axial fretting fatigue set-up at LTDS.

## 2.4. Experimental results

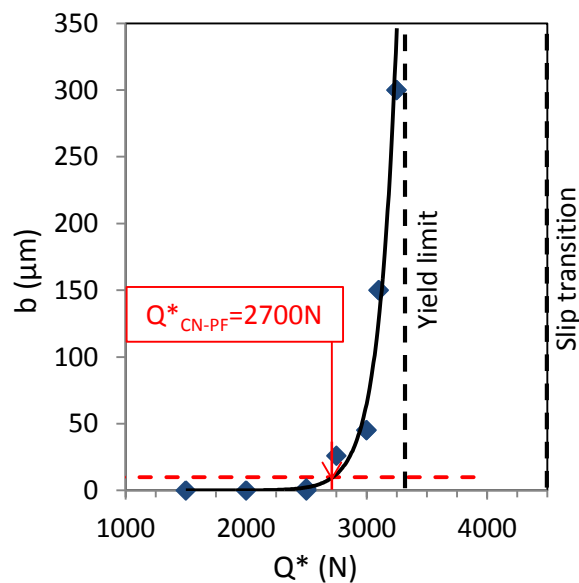
### 2.4.1. Plain fretting test

First, some tests were performed to establish the friction coefficient of the sliding transition. A value  $\mu_t=0.9$  was found, equivalent to the one obtained in a previous study [23]. Then a second set of tests were performed to obtain the crack nucleation condition  $Q^*_{CN}$ .

The experimental methodology to identify  $Q^*_{CN}$  consisted in performing several fretting tests at various tangential fretting force amplitudes  $Q^*$  for  $10^6$  cycles under stabilized partial slip conditions. Cracking identification was performed by optical cross section analyses. It has been shown [24] that in sphere/plane plain fretting contact, maximum crack length is found at the contact border along the fretting axis. Thus fretting scars were cut a bit before the middle plane. The section was polished to a mirror state to observe the desired plane (Fig. 2). Then it was observed with an optical microscope and the maximum projected crack length of the plane measured (Fig. 4a).



(a)



(b)

Figure 4: (a) Observation and measurement of crack length with optical microscope ( $R=200\text{mm}$ ,  $P=5000\text{N}$ ,  $Q^*=2700\text{N}$ ,  $10^6$  cycles). (b) Identification of crack nucleation condition ( $b_{CN}=10\mu\text{m}$ ) under plain fretting loading ( $R=200\text{mm}$ ,  $P=5000\text{N}$ ,  $10^6$  cycles).

All the projected crack lengths measured with the above method were plotted as a function of the related tangential force amplitude (Fig. 4b). With this representation, critical crack nucleation condition  $Q^*_{CN}$  which generates a  $10\mu\text{m}$  crack length was extrapolated for the studied conditions ( $R=200\text{mm}$ ,  $P=5000\text{N}$ ,  $N=10^6$  cycles). We found  $Q^*_{CN-PF}=2700\text{N}$ . For smaller force, no crack nucleation is considered, for larger force a cracking risk is assumed. Note that all the crack nucleation conditions expertised, corresponded to fretting loadings lower than the yield stress condition. This confirmed that the studied crack nucleation condition was related to macroscopic elastic configuration.

2.4.2. Collinear fretting fatigue tests results

All fretting fatigue were performed keeping constant contact loading  $R=200\text{mm}$ ,  $P=5000\text{N}$  and fatigue loading:  $\sigma_{F,max}=400\text{MPa}$ ,  $\sigma_{F,min}=320\text{MPa}$  leading to a fatigue stress ratio of  $R_\sigma = \sigma_{F,min}/\sigma_{F,max}=0.8$ . It is important to note that in this test, the fatigue sample is fixed at the top and the fatigue force is applied through the bottom of the sample (Fig. 2). This dissymmetry promotes a unidirectional strain mismatch in the contact zone, which induces a shift of the stick zone (Fig. 5). This shift is quantified by an “eccentricity” length ‘e’ which need to be considered in the stress analysis. Note that normal force was applied after the application of the mean fatigue stress so that the resulting stress variation corresponded to the fatigue stress amplitude.

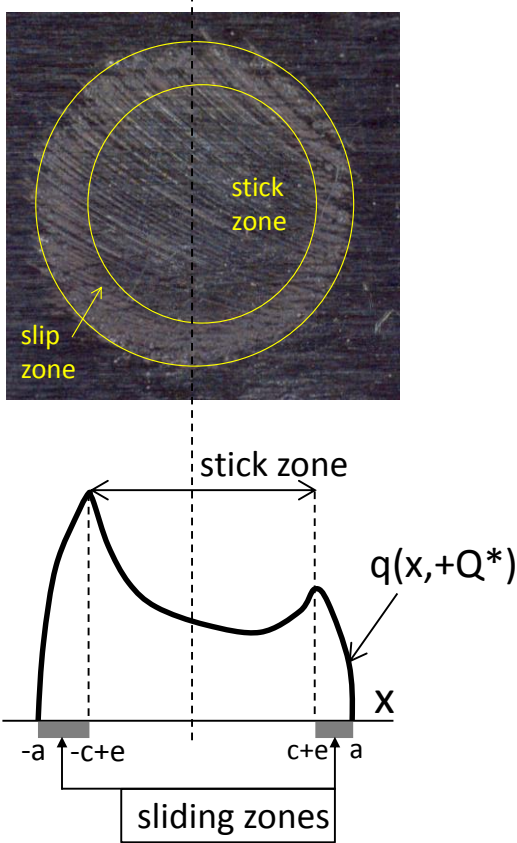


Figure 5: Eccentricity in collinear fretting fatigue

Short experiments were first performed to measure this value. A value of about  $e=60\mu\text{m}$  was found which is a bit larger than the numerical estimation provided by Navarro et Dominguez [25]:

$$e = \frac{4 \times \sigma_{F,a} \times a}{\pi \times \mu \times p_0} \times \frac{1}{(1+\nu) \times (4-3\nu)} = 40\mu\text{m} \tag{1}$$

with  $\sigma_{F,a}$  fatigue stress amplitude,  $a_H$  Hertzian contact radius,  $\mu$  coefficient of friction,  $p_0$  maximum contact pressure and  $\nu$  poisson's ratio.

The determination of this value is important according that it induces a dissymmetry of the shear profile inducing an overstressing at the trailing edge. A FEM element analysis with  $\lambda$  40 $\mu$ m mesh size also gave a value of  $e=60\mu$ m. Hence, this value was considered for the latter analytical modelling.

Crack nucleation condition for collinear fretting fatigue,  $Q^*_{CN-FF,0}$ , was not identified with the same method as for plain fretting. Indeed, propagation was so fast that sample either failed before  $10^6$  cycles, or no crack was observed in the contact when the sample did not fail. This behavior can be related to the fact that both fretting and fatigue loadings work together to propagate the crack.

Crack nucleation was thus related to the last unfailed condition at  $10^6$  cycles as shown in Fig. 6. We found  $Q^*_{CN-FF,0}=1375$ N.

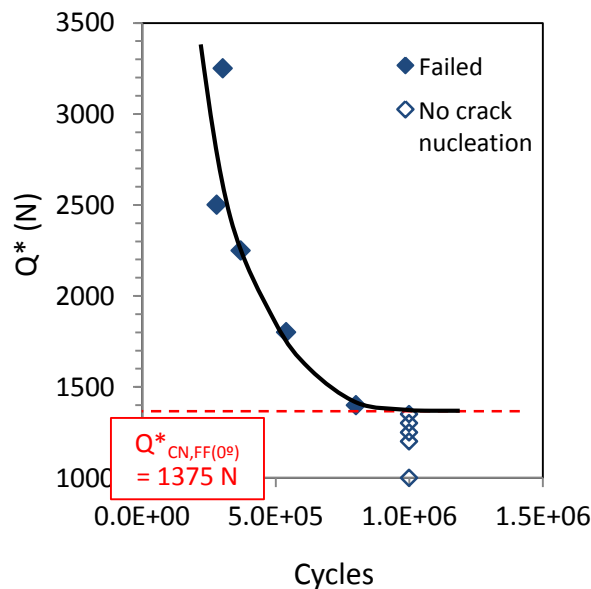


Figure 6: Identification of crack nucleation condition under collinear fretting fatigue loading  $\beta=0^\circ$  ( $R=200$ mm,  $P=5000$ N,  $\sigma_{F,max}=400$ MPa,  $R_\sigma=0.8$ ,  $10^6$  cycles).

It should be noted that  $Q^*_{CN-FF,0}$  was 2 times smaller than  $Q^*_{CN-PF}$ . Besides, cracking failure was systematically observed at the bottom side of the fretting scar (i.e. trailing contact order). These results are consistent with the eccentricity effect, which accentuates the stress state at the trailing side of the contact, inducing a dissymmetrical cracking process and leading to a faster crack nucleation.

#### 2.4.3. Non collinear fretting fatigue tests results

Similar test condition than for collinear configurations were applied:  $R=200$ mm,  $P=5000$ N,  $\sigma_{F,max}=400$ MPa,  $R_\sigma=0.8$ ,  $10^6$  cycles. Crack nucleation investigation was performed for 3  $\beta$ -angles:  $60^\circ$ ,  $75^\circ$  and  $90^\circ$ . Symmetrical fatigue stress was imposed so the central point of the fatigue specimen where the contact was applied remained static. Contrary to collinear tests, this symmetry ensured symmetrical strain mismatch in the contact zone so that no stick zone eccentricity is occurring (Fig. 2). This was confirmed by the surface fretting scars which showed symmetrical stick zones and by the

fact that crack failure was randomly observed either side of the fretting scar (Fig. 7). Fig. 7 illustrates typical cracked fretting scars obtained for  $\beta=60^\circ$  and  $\beta=90^\circ$ . It is interesting to note that crack nucleation seems along the fretting axis. However concerning crack extension, crack path can bifurcate to propagate perpendicularly to the main fatigue stressing (Fig. 2). This interesting aspect will be investigated in future works focusing on crack propagation.

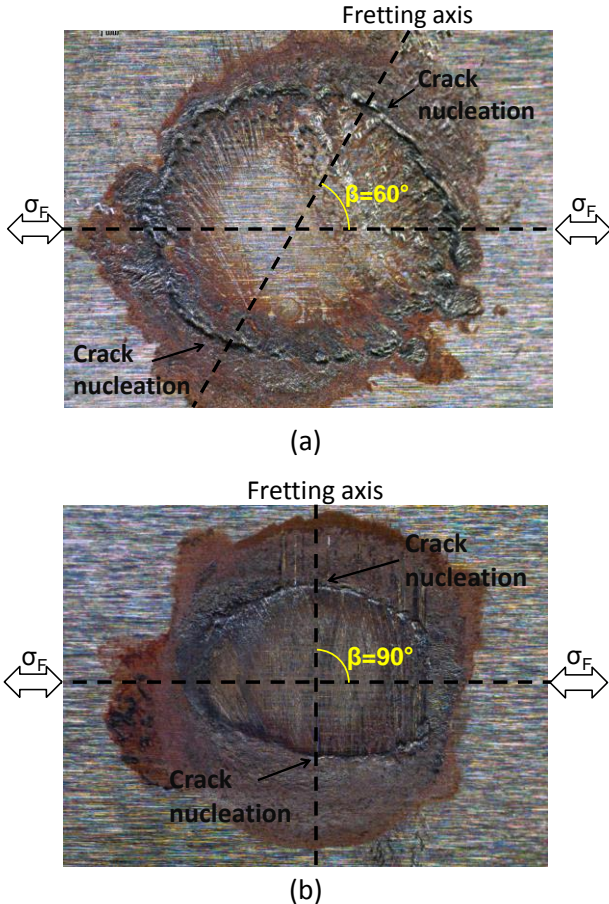


Figure 7: Fretting scars in multiaxial fretting fatigue after  $10^6$  cycles. (a)  $\beta=60^\circ$ ,  $Q^*=2700N$ ; (b)  $\beta=90^\circ$ ,  $Q^*=3100N$ . ( $R=200mm$ ,  $P=5000N$ ,  $\sigma_{F,max}=400MPa$ ,  $R_\sigma=0.8$ ,  $10^6$  cycles).

Another aspect concerns the location of crack nucleation which seems occurring inside the fretted interfaces (Fig. 7). In fact with the crack extension the contact stiffness drastically drops inducing a significant contact area extension. Therefore a crack which initially nucleated at the contact border could appear inside of the fretted surface at the end of the test.

Similar destructive methodology, as used for plain fretting experiments, has been applied to identify the threshold crack nucleation conditions in multiaxial fretting fatigue,  $Q^*_{CN-FF,\beta}$ . Fig. 8 illustrates the methodology for  $\beta=90^\circ$ . For small cracks ( $<30\mu m$ ), as studied for crack nucleation, and for the studied conditions, maximum crack length was always in the middle of the fretting scar along the fretting axis (Fig. 8). Hence, for most tests, only one observation plane was done, in this plane. Tests were running up to  $10^6$  cycles and the obtained crack lengths were reported as a function of the applied tangential force amplitude. Then, assuming  $b_{CN}=10\mu m$ , the corresponding  $Q^*_{CN-FF,\beta}$  were extracted and compiled in Table 2.

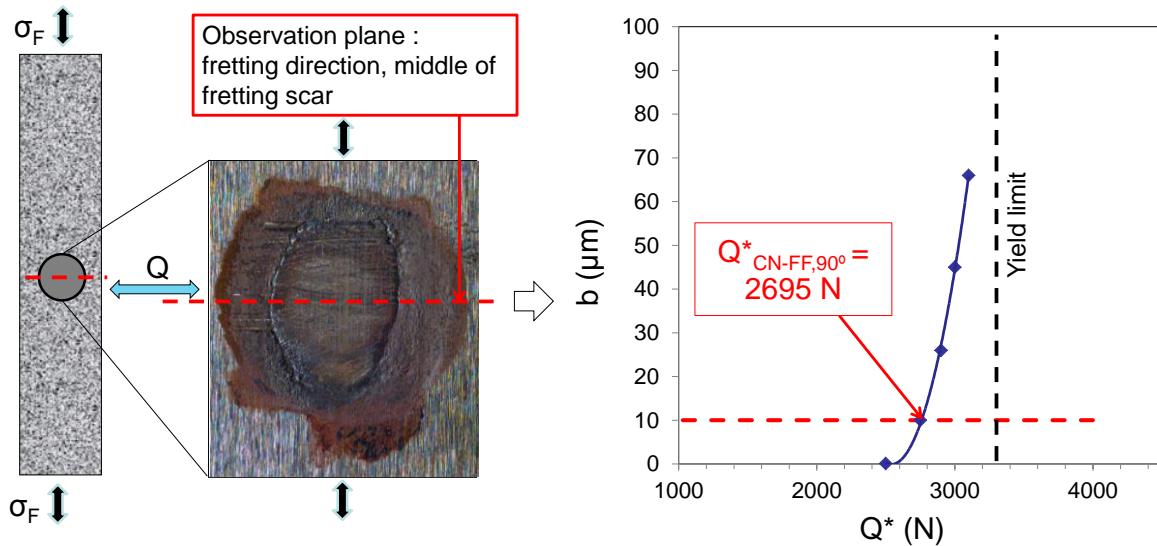


Figure 8: Illustration of the methodology used to identify the crack nucleation of non collinear fretting fatigue experiments ( $R=200\text{mm}$ ,  $P=5000\text{N}$ ,  $\sigma_{F,\text{max}}=400\text{MPa}$ ,  $R_\sigma=0.8$ ,  $10^6$  cycles,  $\beta=90^\circ$ )

Table 2: Crack nucleation conditions; sphere on plane contact with  $R=200\text{mm}$

Name	Test	P (N)	$\sigma_{F,\text{max}}$ (MPa)	$R_\sigma = \sigma_{F,\text{min}}/\sigma_{F,\text{max}}$	$\beta(^{\circ})$	$Q^*_{\text{CN}}$ (N)
$Q^*_{\text{CN-PF}}$	PF	5000	400	0.8	-	$2700 \pm 10$
$Q^*_{\text{CN-FF},0}$	FF	5000	400	0.8	0	$1375 \pm 10$
$Q^*_{\text{CN-MFF},60}$	NCFE	5000	400	0.8	60	$2520 \pm 10$
$Q^*_{\text{CN-MFF},75}$	NCFE	5000	400	0.8	75	$2660 \pm 10$
$Q^*_{\text{CN-MFF},90}$	NCFE	5000	400	0.8	90	$2695 \pm 10$

The crack nucleation conditions obtained for each angle (Table 2) are plotted as a function of angle beta in Fig. 9.  $Q^*_{\text{CN-FF}}$  increases with  $\beta$ . Misaligning fretting and fatigue loadings reduced the stress state. But fatigue loading contributed obviously to the crack nucleation process since the crack nucleation boundary increases as function of  $\beta$ -angle. When comparing those results to  $Q^*_{\text{CN-FF},0}$ , it appears that there is a large gap. The only exception is for  $\beta=90^\circ$ , where  $Q^*_{\text{CN-FF},90} \approx Q^*_{\text{CN-PF}}$  meaning that the fatigue, because of the perpendicularity, had no influence on crack nucleation.

Two questions arise:

- Is this evolution of crack nucleation threshold a consequence of the  $\beta$ -angle or a consequence of the eccentricity that is only found in collinear fretting fatigue?
- Which multiaxial fatigue formalism is the most appropriate to predict such evolution?

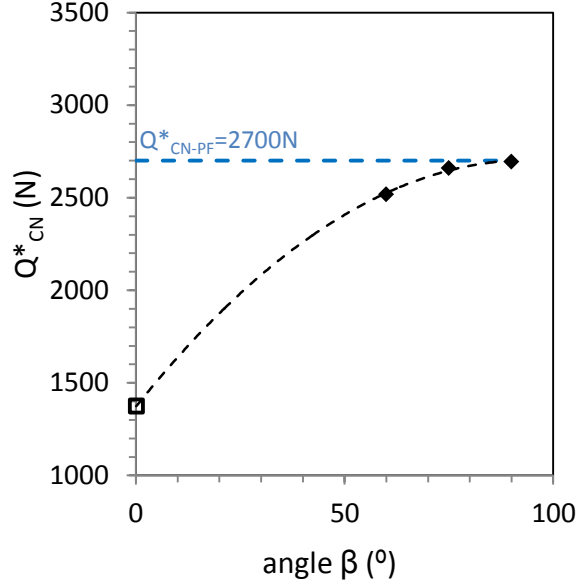


Figure 9: Crack nucleation conditions as functions of angle  $\beta$  ( $R=200\text{mm}$ ,  $P=5000\text{N}$ ,  $\sigma_{F,\text{max}}=400\text{MPa}$ ,  $R_\sigma=0.8$ ,  $10^6$  cycles). ( $\blacklozenge$ ) Non collinear FF crack nucleation conditions (NCCF test: centroid fatigue stress  $\rightarrow$  no eccentricity); ( $\blacksquare$ ) Collinear fretting fatigue crack nucleation condition (FF test: eccentricity).

### 3. Crack nucleation modelling

#### 3.1. Stress field modelling

The sphere/plane partial slip contact is assumed to follow Hertzian hypothesis [2]. The surface loading can be described as a sum of a constant loading induced by the normal force and an alternated shear stress field induced by the cyclic tangential force as described by Mindlin's formalism [2,20]. The surface loading during the fretting cycle is then expressed as the superposition of a constant Hertzian pressure distribution  $p(x)$  and an alternated shear field distribution  $q(x)$ . The loading path is deduced by combining these descriptions with the Hamilton formulation for a full sliding sphere/plane contact [26].

To this contact loading, the bulk fatigue loading is added following again the superposition principle so that:

$$\Sigma_{\text{FF}} = \Sigma_{\text{PF}} + \Sigma(\beta)_{\text{Fatigue}} \quad (2)$$

The fatigue tensor is rotated so that the global fretting fatigue tensor  $\Sigma_{\text{FF}}$  is expressed in the fretting system. The rotated fatigue matrix is as follow:

$$\Sigma(\beta)_{\text{Fatigue}} = \begin{pmatrix} \sigma_F \cos^2 \beta & -\sigma_F \cos \beta \sin \beta & 0 \\ -\sigma_F \cos \beta \sin \beta & \sigma_F \sin^2 \beta & 0 \\ 0 & 0 & 0 \end{pmatrix} \quad (3)$$

For the case where  $\beta=0^\circ$ , eccentricity was taken into account with  $e=60\mu\text{m}$  as detailed previously.

Using this analytical methodology the global stress state under the contact was obtained. Fig. 10a plots on the first row, the computed principal stress  $\sigma_1$  depending on the fretting fatigue loading. For plain fretting, the mapping is obviously symmetrical. For  $\beta=0^\circ$ , the eccentricity leads to a strong stress concentration on the side of the applied fatigue loading. For  $\beta>0^\circ$ , mapping displays the competitiveness between fretting loading and fatigue loading. This tendency is confirmed by the evolution of  $\sigma_1$  along the contact border, as plotted in Fig. 10b for  $\beta=60^\circ$ ,  $\sigma_{1,max}$  being between fretting and fatigue axes.

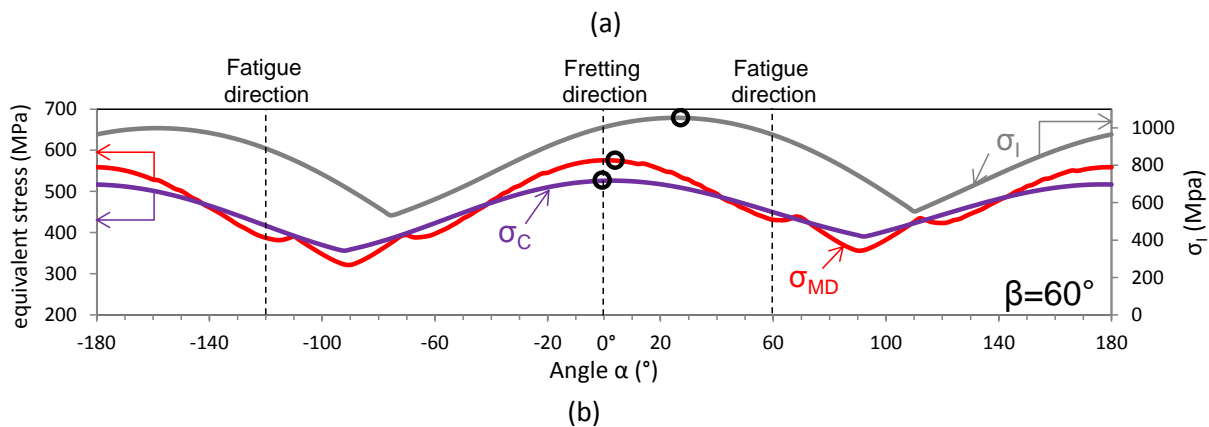
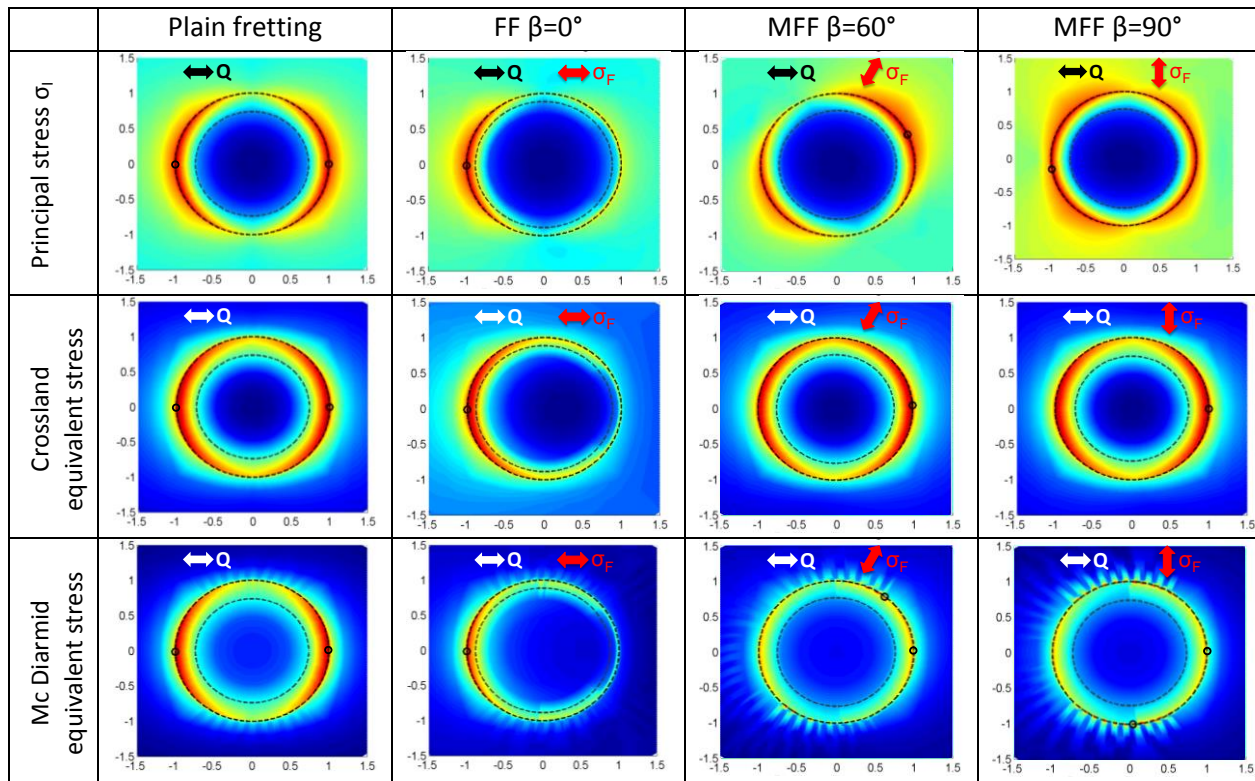


Figure 10: (a) XY mapping of  $\sigma_1$ , Crossland, Mc Diarmid as function of fretting fatigue loading and localization of maximum cracking risk. (b)  $\sigma_1$ , Crossland, Mc Diarmid evolution along the contact border for  $\beta=60^\circ$ . ( $R=200\text{mm}$ ,  $P=5000\text{N}$ ,  $Q^*_{CN}$ ,  $\sigma_{F,max}=400\text{MPa}$ ,  $R_0=0.8$ ,  $10^6$  cycles).

From this stress state, it is possible to study crack nucleation risks using multiaxial fatigue criteria. In the literature, different formulations have been proposed. In this work we focus on four different

approaches: invariant Crossland criterion [27] and Dang Van mesoscopic formulation [28] and critical plane McDiarmid criterion [29] and SWT formulation [30].

### 3.2. Invariant criteria

#### 3.2.1. Crossland

Crossland's multiaxial fatigue criterion expresses cracking risk as a linear combination of the square root of the maximum amplitude of the second invariant of the stress deviator defined by  $\sqrt{J_{2,a}}$ , and the maximum hydrostatic pressure  $\sigma_{H,max}$  [27]:

$$\sigma_C = \sqrt{J_{2,a}} + \alpha \cdot \sigma_{H,max} \quad (4)$$

with

$$\sigma_{H,max} = \max_{t \in T} \left( \frac{1}{3} \text{trace} \left( \underline{\underline{\Sigma}}(t) \right) \right) \quad (5)$$

$$\sqrt{J_{2,a}} = \frac{1}{2} \max_{t_0 \in T} \left\{ \max_{t \in T} \left[ \frac{1}{2} \left( \underline{\underline{S}}(t) - \underline{\underline{S}}(t_0) \right) : \left( \underline{\underline{S}}(t) - \underline{\underline{S}}(t_0) \right) \right]^{1/2} \right\} \quad (6)$$

$$\alpha_C = \frac{\tau_d - \frac{\sigma_d}{\sqrt{3}}}{\frac{\sigma_d}{3}} \quad (7)$$

where  $S$  is the deviatoric part of  $\Sigma$ ,  $\sigma_d$  the traction-compression fatigue limit and  $\tau_d$  the torsional fatigue limit. Cracking risk can then be estimated by comparing the equivalent Crossland stress to the torsional fatigue limit  $\tau_d$  so that the non-cracking condition is expressed by:

$$\sigma_C \leq \tau_d \quad (8)$$

Fig. 10 plots mapping of Crossland Criterion on the XY surface for various  $\beta$  angles. It is interesting to note that maximum cracking risk is always on fretting axis whatever the  $\beta$ -angle which confirms the experimental observations.

#### 3.2.2. Dang Van

Dang Van fatigue approach considers crack nucleation on the grain which presents an easy slip band direction with regard to the macroscopic loading direction [28]. Surrounded by an elastic matrix, the grain will first undergo a plastic deformation before reaching an elastic shakedown state. The elastic stabilization and the initial plastic hardening with which it is associated correspond to the introduction of a local residual stress tensor  $\rho^*$ . The stabilized local stress tensor  $\hat{\sigma}(t)$  loading imposed on the grain on which the fatigue analysis must be performed is consequently defined as the sum of the macroscopic  $\Sigma(t)$  loading and the stabilized residual stress  $\rho^*$ :

$$\hat{\sigma}(t) = \Sigma(t) + \rho^* \quad (9)$$

From the local stress tensor  $\hat{\sigma}(t)$ , the two microscopic stress components, shear stress  $\hat{\tau}$  and hydrostatic pressure  $\hat{\sigma}_H$  are determined. The model assumes that there is a sufficient number of

grain in the representative volume so that at least one grain displays an easy slip band collinear to the tresca value of the microscopic stress tensor [28]:

$$\hat{t} = \frac{1}{2} \max(Tresca(\hat{\sigma}(t))) \quad (10)$$

In consequence the formulation of the Dang Van criterion can be related to an equivalent microscopic stress invariant formulation with Dang Van local cracking risk being expressed by:

$$\sigma_{DV} = \hat{t} + \alpha_{DV} \hat{\sigma}_H \quad (11)$$

With

$$\alpha_{DV} = \frac{\tau_d - \sigma_d/2}{\sigma_d/3} \quad (12)$$

The non-cracking condition is expressed by:

$$\sigma_{DV} \leq \tau_d \quad (13)$$

### 3.3. Critical plane criteria

#### 3.3.1. SWT

The SWT [30] parameter, called  $\Gamma$ , is the maximum value of the product of the normal strain amplitude  $\varepsilon_a$ , and the maximum normal stress  $\sigma_{max}$  applied to the material. All  $n$  plane orientations of the 3D space are investigated to obtain the maximum value of the  $\Gamma$  parameter. Indeed according to SWT approach, crack initiates on the plane where  $\Gamma$  parameter is maximum:

$$\Gamma = \max_n [\sigma_{max}(n) \times \varepsilon_a(n)] \quad (14)$$

and there is a cracking risk when:

$$\Gamma \geq \Gamma_{CN} \quad (15)$$

where  $\Gamma_{CN}$  is the critical SWT value related to the material at  $10^6$  cycles. For numerous steel alloys,  $10^6$  cycles is close to the fatigue limit particularly if, as in the present study, crack nucleation is considered. Thus it is possible to derive the following formulation [31]:

$$\Gamma_{CN} = \sigma_d^2 / E \quad (16)$$

#### 3.3.2. McDiarmid

The McDiarmid critical plane fatigue criterion was identified from numerous fatigue experiments. It assumes that a crack initiates on the critical plane  $n^*$  where the shear stress amplitude is the greatest (i.e.  $n^* : \max_n(\tau_a(n))$ ) [29]. The McDiarmid equivalent stress state on this plane is then expressed by:

$$\sigma_{MD} = \left\{ 1 - \left[ \frac{\sigma_{n,m}(n^*)}{\sigma_u/2} \right] \right\}^{-1/2} \tau_a(n^*) + \alpha_{MD} \cdot \sigma_{n,a}(n^*)^{3/2} \quad (17)$$

with

$$\alpha_{MD} = \frac{\tau_a - \sigma_d/2}{(\sigma_d/2)^{3/2}} \quad (18)$$

where  $\tau_a(n^*)$  and  $\sigma_{n,X}(n^*)^{3/2}$  are respectively the shear stress amplitude and normal stress relative to the plane of maximum shear stress amplitude (X=a : amplitude value, X=m: mean value). There is a cracking risk when:

$$\sigma_{MD} \geq \tau_d \quad (19)$$

Fig. 10 plots mapping of McDiarmid Criterion on the XY surface for various  $\beta$  angles. As for Crossland criterion, maximum cracking risk is always close to fretting axis. For  $\beta=60^\circ$ , Fig. 10b shows that the maximum cracking risk may differ a little from the fretting axis. This will be studied in depth in the coming paragraphs.

### 3.4. Stress gradient effect and calibrations

Fig. 11 plots the subsurface distribution of the Crossland equivalent stress related to the crack nucleation condition defined for the plain fretting crack nucleation condition ( $P=5000N$ ,  $Q^*_{CN-PF}=2700N$ ). The distribution was characterized by severe stress gradients. Other criteria showed similar distributions. These stress gradients lead to over-estimation of cracking risk at the hot spot (i.e., the top surface contact border in fretting fatigue). To palliate this problem, non-local fatigue stress analyses are required as explained in the introduction.

Three different strategies were considered here and compared with each other. The first one consists in computing a mean stress loading path averaged over a representative process volume domain surrounding the fatigue hot spot [13,24]. A key aspect of this approach is the determination of the representative material volume, usually defined by its half cubic length scale ( $\ell_v$ ). The second strategy consists in averaging the loading path over a line of length  $\ell_L$  instead of a volume [13]. The last strategy, extensively applied in academic research, is based on the critical distance method developed by Taylor and co-authors [14] and Araujo's research group [12]. This approach consists in considering the equivalent fatigue stress at a critical distance ( $\ell_D$ ) from the hot spot stress.

Whichever the method, prediction will depend on the length scale variable ( $\ell_v$ ,  $\ell_L$  or  $\ell_D$ ) used to compute the representative stress state to be compared to the material fatigue data to predict the cracking risk. A reverse strategy was applied to calibrate for each criterion, the 3 length scale variables on the plain fretting crack nucleation condition. Fig. 11 shows an example of the method for Crossland criterion. It shows that  $\sigma_c = \tau_d$  if  $\ell_{D,c} = 22\mu m$ . Likewise,  $\ell_v$  and  $\ell_L$  were identified when the respective averaged equivalent stress were equal to  $\tau_d$ .

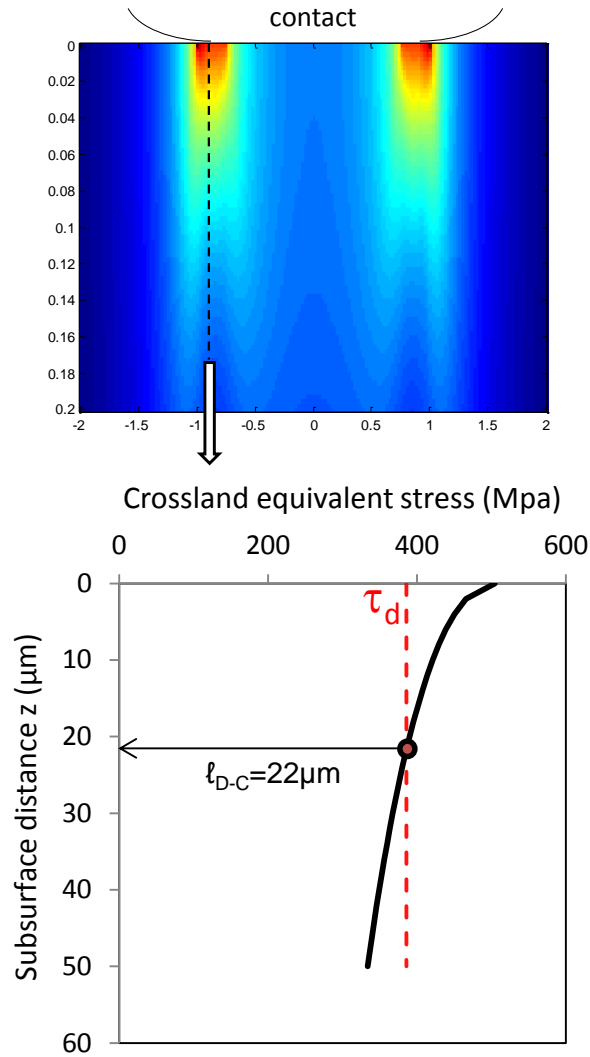


Figure 11: Identification of critical distance  $l_{D-C}$  from subsurface Crossland distribution ( $R=200\text{mm}$ ,  $P=5000\text{N}$ ,  $Q^*=2700\text{N}$ ).

Table 3 gathers all the identified length scale variables with respect to the four multiaxial fatigue criteria.

Table 3: length scales identified from plain fretting crack nucleation ( $R=200\text{mm}$ ,  $P=5000\text{N}$ ,  $Q^*=2700\text{N}$ ,  $10^6$  cycles) condition for non-local analyses

	$l_D$ (μm)	$l_L$ (μm)	$l_v$ (μm)
Crossland (C)	22	54	98
Dang Van (DV)	35	88	162
SWT	30	74	138
McDiarmid (MD)	33	82	132

### 3.5. Results

#### 3.5.1. Crack nucleation prediction results

Using the various length scales identified in Table 3, fretting fatigue crack nucleation can now be predicted. To better quantify predictions and compare all 12 possible criterion/length scale combinations, two indices were introduced:

- %E, mean absolute error, estimates the global error of prediction versus the experimental condition:

$$\%E = \frac{1}{N} \sum_{i=1}^N \sqrt{(VQ)^2} \quad \text{where } VQ = \frac{Q_{th}^* - Q_{exp}^*}{Q_{exp}^*} * 100 \quad (20)$$

- %SD, standard deviation, provides a relative estimation of dispersion:

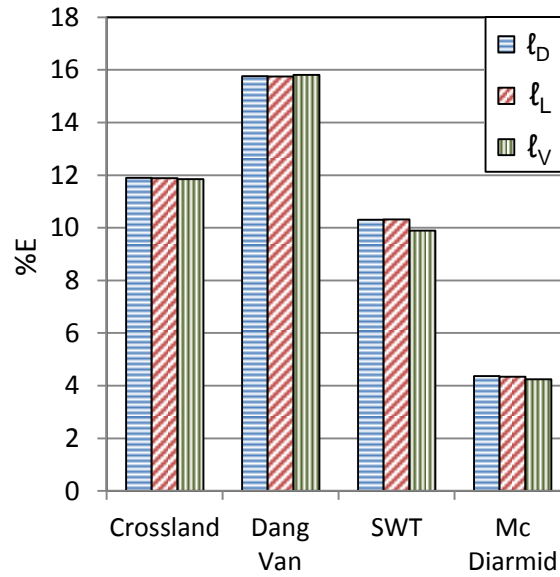
$$\%SD = \sqrt{\frac{\sum (VQ - \overline{VQ})^2}{(N-1)}} \quad \text{where } \overline{VQ} = \frac{1}{N} \sum_{i=1}^N VQ \quad (21)$$

With  $N = 4$  for all four fretting fatigue angle studied  $\beta=0^\circ, 60^\circ, 75^\circ$  and  $90^\circ$  and considering the experimental crack nucleation conditions of Table 2.

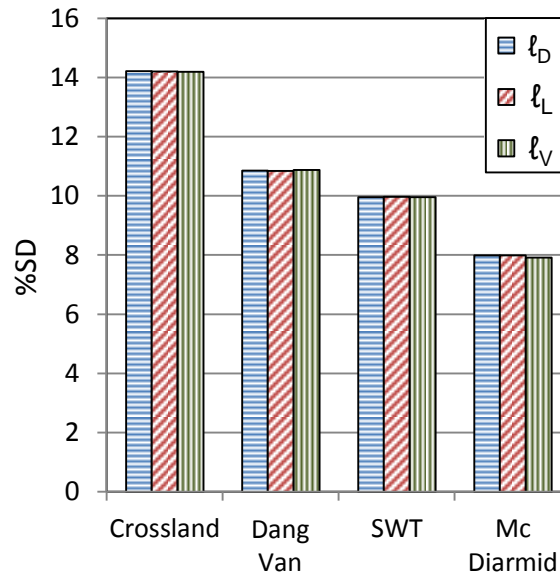
Fig. 12 plots %E and %SD as functions of multiaxial fatigue criteria and non-local analysis methods.

#### 3.5.2. Comparison between length scale approaches

Whatever the length scale approach used (i.e. crack nucleation process volume, crack nucleation process line and critical distance method), indices %E and %SD display quasi equivalent results which suggests that they lead to similar prediction of crack nucleation threshold. These results follow the observation of Fouvry et al. for collinear fretting fatigue, which is that none of the approach used can be preferred to describe the stress gradient effect induced by the fretting loading [13]. We confirm this tendency for this multiaxial non collinear fretting fatigue investigation.



(a)



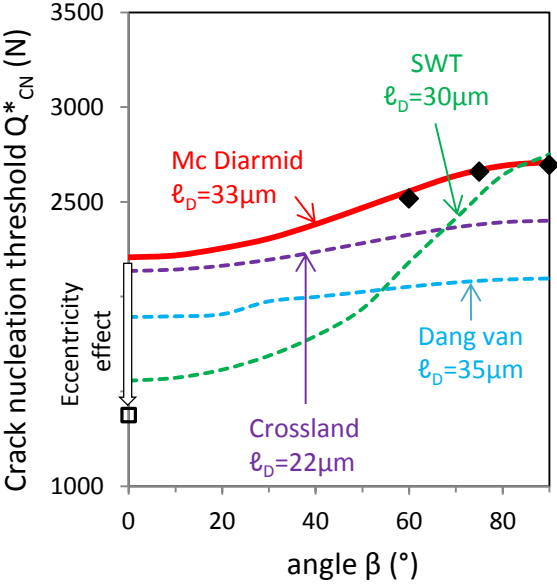
(b)

Figure 12: (a) mean absolute error and (b) standard deviation over the 4 fretting fatigue loadings at 4 different  $\beta$  angles considering 12 various criterion/length-scale combinations. ( $P=5000N$ ,  $\sigma_{F,max}=400MPa$ ,  $R_\sigma=0.8$ ,  $10^6$  cycles).

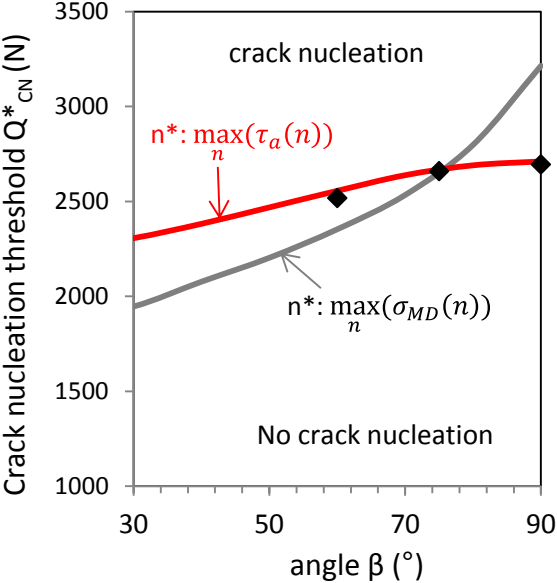
### 3.5.3. Comparison between multiaxial fatigue criteria

Contrary to length scale approaches, the non collinear fretting fatigue loading allows to discriminate between multiaxial fatigue criteria. Four different criteria were considered: Crossland, Dang Van, SWT and McDiarmid. Crossland and Dang Van led to the worst results (Fig. 12 and Fig. 13a). This suggests that stress invariant criteria seem unable to catch threshold evolution with an angle  $\beta$  between fretting and fatigue loadings.

Critical plane criteria provided better prediction and McDiarmid formulation gave the best results. Indeed with %E=4% and %SD=8%, this criterion led to minimal error and dispersion compared to experimental crack nucleation conditions.



(a)



(b)

- ◆ : Non collinear FF crack nucleation conditions (centroid fatigue stress → no eccentricity)
- ◻ : Collinear fretting fatigue crack nucleation condition (eccentricity)

Figure 13: (a) Comparison between multiaxial fatigue criteria for crack nucleation threshold prediction versus experimental crack nucleation conditions. (b) Predicted Mc Diarmid crack nucleation boundaries with (—) original “maximum shear plane” formulation for critical plane  $n^*$  ( $\max_n(\tau_a(n))$ ), or with (—) maximum equivalent stress for critical plane ( $\max_n(\sigma_{MD}(n))$ ). (R=200mm, P=5000N,  $\sigma_{F,max}$ =400MPa,  $R_\sigma$ =0.8,  $10^6$  cycles).

This tendency was confirmed by comparing the predicted threshold tangential force amplitude  $Q_{CN-FF}^*$ , considering the critical distance method, versus the non collinear fretting fatigue experiments (Fig. 13a). Note that the simulations were done assuming centroid fatigue stress condition (i.e. without eccentricity correction) like imposed using non collinear fretting fatigue test. This explains the difference with double actuator collinear experimental results ( $\beta=0^\circ$ ) for which no centroid fatigue stress was imposed so that a significant eccentricity effect occurred.

The comparison clearly underlines the very good predictions provided by McDiarmid critical plane criterion (Fig. 13a). By contrasts all the invariant formulations significantly underestimate the threshold tangential fretting force amplitude inducing over conservative predictions.

One remaining question was the definition of the critical plane for application of McDiarmid critical plane multiaxial fatigue criterion. Indeed original formula, as described in section 3.3.2, considers the plane of maximum shear stress amplitude as critical plane (i.e.  $n^*: \max_n(\tau_\alpha(n))$ ) [29]. However other criteria, such as SWT, consider the plane of maximum criterion as critical plane. Similar formulation was considered with McDiarmid criterion (i.e.  $n^*: \max_n(\sigma_{MD}(n))$ ) still considering the critical distance method to address the stress gradient effect (Fig. 13b).

The comparison with experiments on Fig. 13b confirms that original Mc Diarmid formulation, which considers the plane of maximum shear stress amplitude for critical plane, is the best approach for predicting fretting fatigue crack nucleation.

## 4. Discussion

$\beta$ -angle between fretting and fatigue loadings allowed discriminating between multiaxial fatigue criteria and identified McDiarmid criterion as the most pertinent approach to predict crack nucleation for such multiaxial loading. Using this criterion, the influence of  $\beta$ -angle on crack nucleation is now examined focusing on two aspects: the influence of  $\beta$ -angle at constant fatigue loading and the influence of variable fatigue stress ratio.

### 4.1. Parametric study on $\beta$ -angle

Conventional collinear fretting fatigue leads to localized crack nucleation at contact border along fretting axis. We have shown experimentally that multiaxial fretting fatigue lead to quasi-similar behavior (see section 2.4.2). However, no angle were tested between  $0^\circ < \beta < 60^\circ$ . Introduction of an angle  $\beta$  between fretting and fatigue loading may induce a crack nucleation outside of the fretting axis and somewhere between fretting axis and fatigue axis (Fig. 10). To answer this question, parametric study was performed, considering constant fatigue load ( $\sigma_{F,max}=400\text{MPa}$ ,  $R_\sigma=0.8$ ), to identify the maximum cracking risk localization and orientation as a function of  $\beta$ -angle.

Surface crack nucleation localization is characterized by the radial distance from the center of the fretting scar ( $r$ ) and the  $\alpha$ -angle versus the  $x$  fretting axis (see scheme on Fig. 14). For instance, when  $r/a=1$ , maximum cracking risk is on the contact border and when  $\alpha=0$ , it is along the median fretting axis. Fig. 14 plots the evolution of both parameters as function of  $\beta$ -angle.  $r/a$  remains constant at  $r/a=1$ . Whatever is the  $\beta$ -angle, maximum cracking risk is always at contact border. Angle  $\alpha$  evolves with  $\beta$ . However its value stays relatively low: below  $10^\circ$ .

The critical plane orientation of maximum cracking risk is characterized by two angles,  $\theta$  and  $\varphi$ , as schematized on Fig. 14.  $\theta$  is the angle between the normal to the critical plane and the surface plane

( $x,y$ ) and  $\varphi$  is the angle of the critical plane versus the radial direction. Fig. 14 plots the evolution of both parameters as function of  $\beta$ -angle. Both remain constant whatever  $\beta$ -angle, with a critical plane systematically oriented at  $45^\circ$  below the surface ( $\theta=45^\circ$ ) and tangent to the contact border ( $\varphi=90^\circ$ ). Considering that  $\alpha$  is close to zero, maximum cracking risk can be assumed to be at contact border along the fretting axis  $x$ . This result justifies that fretting loading is the driving parameter of crack nucleation. In addition it allows for faster calculi limiting the critical plane analysis to the single X-Z media subsurface fretting plane.

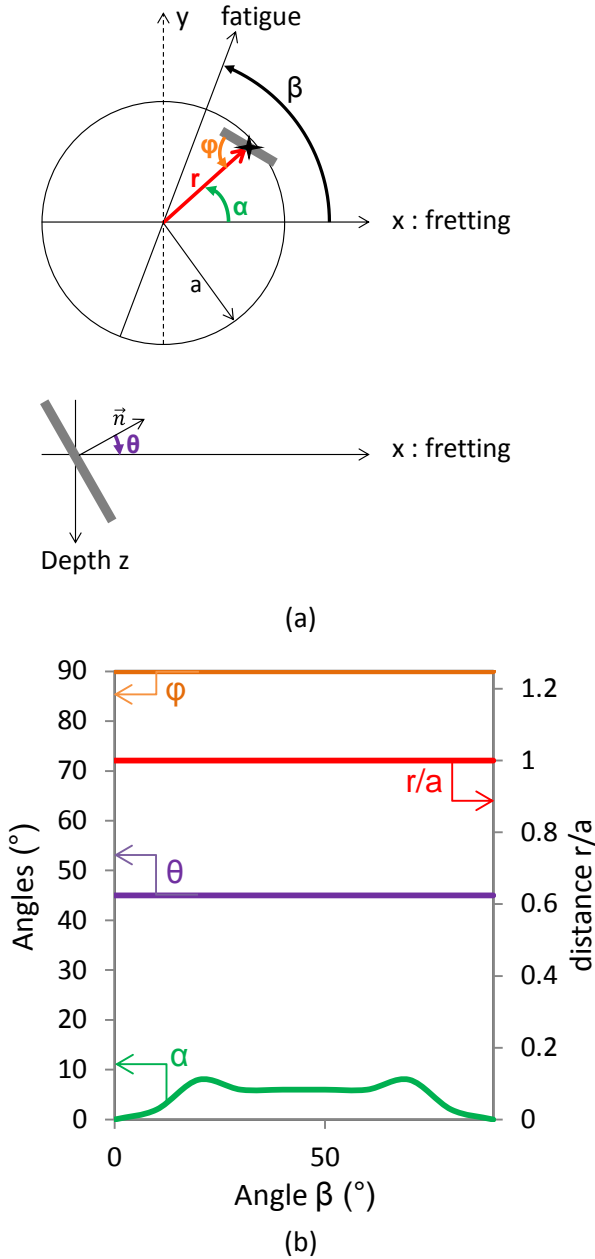


Figure 14: (a) Definition of parameters  $r$ ,  $\alpha$ ,  $\theta$  and  $\varphi$  for crack nucleation localization and critical plane orientation. (b) Evolution of the four parameters as functions of  $\beta$ . ( $R=200\text{mm}$ ,  $P=5000\text{N}$ ,  $\sigma_{F,\text{max}}=400\text{MPa}$ ,  $R_\sigma=0.8$ ).

#### 4.2. Parametric study on fatigue stress ratio effect

The former  $\beta$  angle analysis was done for a constant fatigue stress condition amplitude which was low ( $R_\sigma=0.8$ ) comparatively to the fretting stressing. This may explain the dominating influence of the contact stress regarding the crack nucleation location. To investigate this aspect, fatigue stress ratio was varied from  $R_\sigma=-1$  to  $R_\sigma=1$  while keeping the maximum fatigue stress constant  $\sigma_{F,max}=400\text{MPa}$ . The crack nucleation tangential force threshold  $Q^*_{CN}$  for 3  $\beta$ -angles is plotted in Fig. 15a as a function of the fatigue stress ratio  $R_\sigma$ . The corresponding crack nucleation parameters  $\alpha$ ,  $r/a$ ,  $\theta$  and  $\varphi$  were also identified. The analysis confirmed that  $r/a$ ,  $\theta$  and  $\varphi$  remains constant at respectively 1,  $45^\circ$  and  $90^\circ$  whatever the  $\beta$ -angle and fatigue stress ratio  $R_\sigma$ . Only angle  $\alpha$  varied as shown in Fig. 15b where the evolution of  $\alpha$ -angle is plotted versus  $R_\sigma$  for 5  $\beta$ -angle conditions.

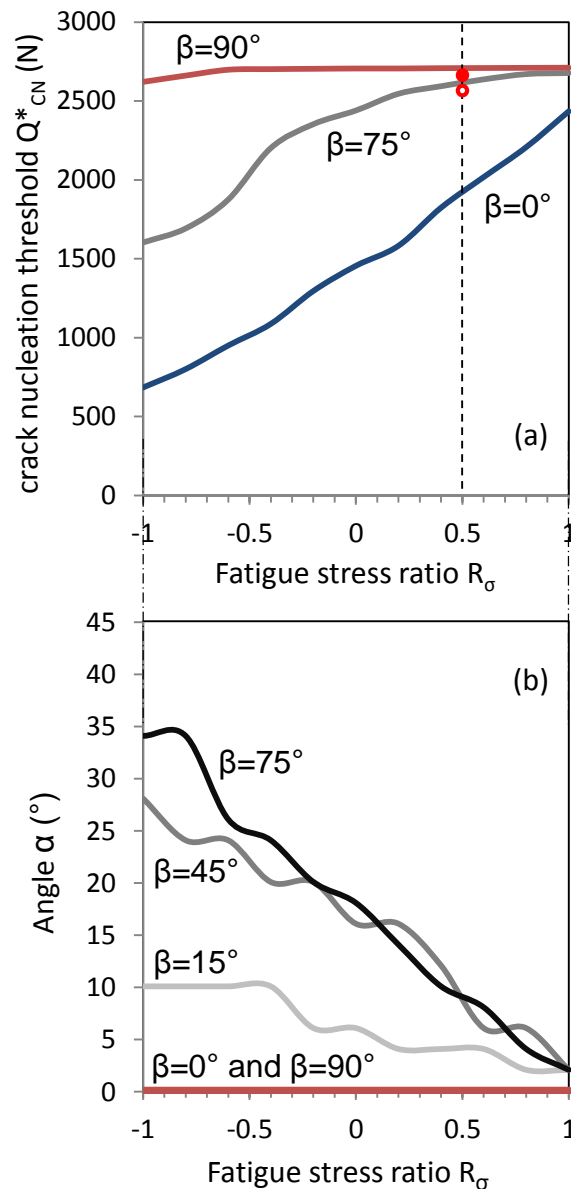


Figure 15: (a) evolution of crack nucleation threshold  $Q^*_{CN}$  as a function of the fatigue stress ratio  $R_\sigma$ .

Comparison with experiments at  $10^6$  cycles for  $\beta=75^\circ$ ; ●: crack nucleation ( $b=50\mu\text{m}$ ); ○: no crack nucleation. (b) Related evolution of the  $\alpha$ -angle with the x fretting axis direction where the first crack is nucleated ( $r/a=1$ ,  $\theta=45^\circ$  and  $\varphi=90^\circ$ ). ( $R=200\text{mm}$ ,  $P=5000\text{N}$ ,  $\sigma_{F,max}=400\text{MPa}$ ).

For  $0^\circ < \beta < 80^\circ$ ,  $\alpha$  angle increases quasi-linearly when  $R_\sigma$  decreases. The slope of such linear increase depends on angle  $\beta$ : the larger the  $\beta$ -angle, the larger the slope. Hence by increasing the fatigue cyclic stress, the relative influence of fatigue loading compared to fretting is increasing so that the location of crack nucleation is becoming closer to the fatigue direction.

It is surprising to note that for  $\beta=90^\circ$ ,  $\alpha$ -angle equals zero like for collinear condition ( $\beta=0^\circ$ ). This may be explained by the fact that for  $\beta=90^\circ$ , the fatigue stress is perpendicular to the fretting one so that the two contributions cannot be added. Crack will be governed either by fatigue stress if the latter is high enough or by fretting like observed in the present investigation.

These tendencies are clearly confirmed by the  $Q_{CN}^*$  evolutions (Fig. 15a). For  $\beta=0^\circ$  both fatigue and fretting stress are collinear so their contributions can be added which can explain a quasi-linear decrease of the fretting  $Q_{CN}^*$  contribution with the increase of  $R_\sigma$  ratio (i.e. increase of fatigue stress amplitude).

For  $\beta=90^\circ$ , fretting and fatigue are perpendicular so their respective contributions cannot be added which explains that whatever the fatigue stress amplitude (i.e.  $R_\sigma$ ), the crack nucleation is related to a constant  $Q_{CN}^*$  fretting loading. This conclusion is fully consistent with the fact that for  $\beta=90^\circ$  the obtained tangential force ( $Q_{CN-FF,90}^*$ ) was equivalent to the plain fretting limit: ( $Q_{CN-PF}^*$ ) (Fig. 9). It demonstrates that when  $\beta=90^\circ$ , fatigue stressing have no effect on fretting fatigue crack nucleation.

For intermediate condition ( $\beta=75^\circ$ ), both fatigue and fretting stress are partly combined which promotes a sigmoid evolution where for larger  $R_\sigma$  (i.e. smaller fatigue stress amplitude), the  $Q_{CN}^*$  fretting threshold converges to the orthogonal  $\beta=90^\circ$  configuration. Note that first experiments tend to confirm this tendency (Fig. 15b).

This result is very important according that using a very basic approach it allows quantifying the relative influence of fatigue stress regarding fretting fatigue crack nucleation behavior.

## 5. Conclusion

A new non-collinear fretting fatigue test, which allows applying non collinear fretting and fatigue loadings, has been developed. Using this innovative test device combined with representative 3D elastic modelling, it was possible for the first time to discriminate the performance between multiaxial strategies. From this investigation it could be concluded that stress invariant criteria (Crossland & Dang Van) seemed unable to catch threshold evolution with a  $\beta$ -angle between fretting and fatigue loadings. We showed that original McDiarmid formulation, which considers the plane of maximum shear stress amplitude for critical plane, was the best criterion for predicting fretting fatigue crack nucleation.

For medium cyclic fatigue stress condition compared to fretting loading like presently investigated, we concluded that crack nucleates systematically along the median x fretting axis ( $\alpha \approx 0$ ) whatever the  $\beta$ -misalignment angle. This first crack was also systematically tangential to the contact scar and oriented at  $45^\circ$  toward the subsurface. For such conditions the fatigue stress analysis can be restricted to the XZ plane, which limits the computation time compared to a full 3D analysis. However, increasing the cyclic fatigue stress by varying the  $R_\sigma$  fatigue stress ratio, we showed that crack nucleation location (i.e.  $\alpha$ -angle) will be closer to the fatigue loading direction. Only exception was  $\beta=90^\circ$ , for which fretting and fatigue are perpendicular and cannot be added so fatigue stressing has no influence on crack nucleation. Nevertheless this result showed that it should be possible to quantify the relative influence of the fatigue stress versus the fretting stressing towards crack

nucleation, using this on-collinear set-up. Another perspective of this work is to look at the crack propagation path which bifurcates towards the fatigue stress direction to study the influence of fatigue and fretting in the propagation phase (Fig. 2).

## References

- [1] D.A. Hills, D. Nowell, *Mechanics of Fretting Fatigue*, Wear. (1994).
- [2] K.L. Johnson, *Contact Mechanics*, Cambridge University press, 1985.
- [3] J. Madge, S. Leen, P. Shipway, A combined wear and crack nucleation–propagation methodology for fretting fatigue prediction, *Int. J. Fatigue*. 30 (2008) 1509–1528.
- [4] S. Garcin, S. Fouvry, S. Heredia, A FEM fretting map modeling: Effect of surface wear on crack nucleation, *Wear*. 330-331 (2015) 145–159.
- [5] C. Petiot, L. Vincent, K. Dang Van, N. Maouche, J. Foulquier, B. Journet, An analysis of fretting-fatigue failure combined with numerical calculations to predict crack nucleation, *Wear*. 183 (1995) 101–111.
- [6] M.P. Szolwinski, T.N. Farris, *Mechanics of fretting fatigue crack formation*, *Wear*. 98 (1996) 93–107.
- [7] S. Fouvry, K. Elleuch, G. Simeon, Prediction of crack nucleation under partial slip fretting conditions, *J. Strain Anal.* 37 (2002) 549–564.
- [8] H. Neuber, *Theory of notch stresses: principles for exact calculation of strength with reference to structural form and material*, 2nd ed., Springer Verlag, Berlin, 1958.
- [9] R.E. Peterson, *Notch-sensitivity*, G. Sines, *Metal fatigue*, McGraw Hill, New York, 1959.
- [10] S. Fouvry, P. Kapsa, L. Vincent, A multiaxial fatigue analysis of fretting contact taking into account the size effect, *ASTM STP*. 1367 (2000) 167–182.
- [11] J.A. Araújo, D. Nowell, R.C. Vivacqua, The use of multiaxial fatigue models to predict fretting fatigue life of components subjected to different contact stress fields, *Fatigue Fract. Eng. Mater. Struct.* 27 (2004) 967–978.
- [12] J.A. Araújo, D. Nowell, The effect of rapidly varying contact stress fields on fretting fatigue, *Int. J. Fatigue*. 24 (2002) 763–775.
- [13] S. Fouvry, K. Kubiak, Development of a fretting–fatigue mapping concept: The effect of material properties and surface treatments, *Wear*. 267 (2009) 2186–2199.
- [14] D. Taylor, Geometrical effects in fatigue: a unifying theoretical model, *Int. J. Fatigue*. 21 (1999) 413–420.
- [15] H. Kitagawa, S. Takahashi, Application of fracture mechanics to very small cracks or the cracks in the early stage, *Am. Soc. Met.* (1976) 627–630.
- [16] C. Gandiolle, S. Fouvry, Stability of critical distance approach to predict fretting fatigue cracking: a “ $\ell_{opt}$ - $b_{opt}$ ” concept, *Int. J. Fatigue*. 82 (2016) 199–210.
- [17] A. Galtier, PhD thesis, ENSAM BORDEAUX, 1993.
- [18] G. Henaff, HDR thesis, Université de Poitiers, 1997.
- [19] S. Fouvry, H. Gallien, B. Berthel, From uni- to multi-axial fretting-fatigue crack nucleation: Development of a stress-gradient-dependent critical distance approach, *Int. J. Fatigue*. 62 (2014) 194–209.
- [20] R.D. Mindlin, H. Deresciewicz, Elastic sphere in contact under varying oblique forces, *J. Appl. Mech.* 75 (1953) 327–344.
- [21] D.A. Hills, *Mechanics of fretting fatigue*, *Wear*. 175 (1994) 107–113.
- [22] J. Meriaux, S. Fouvry, K.J. Kubiak, S. Deyber, Characterization of crack nucleation in TA6V under fretting-fatigue loading using the potential drop technique, *Int. J. Fatigue*. 32 (2010) 1658–1668.
- [23] M.C. Baietto, E. Pierres, a. Gravouil, B. Berthel, S. Fouvry, B. Trolle, Fretting fatigue crack growth simulation based on a combined experimental and XFEM strategy, *Int. J. Fatigue*. 47 (2013) 31–43.
- [24] S. Fouvry, P. Kapsa, F. Sidoroff, L. Vincent, Identification of the characteristic length scale for fatigue cracking in fretting contacts, *J. Phys. IV JP*. 8 (1998) pp. Pr8–159–Pr8–166.
- [25] C. Navarro, J. Dominguez, Contact conditions and stresses induced during fretting fatigue, *Trans. Eng. Sci.* 24 (1999) 2–8.
- [26] G.M. Hamilton, Explicit equations for the stresses beneath a sliding spherical contact, *Proc. Inst. Mech. Eng.* 197C (1983) 53–59.
- [27] B. Crossland, Effect of large hydrostatic pressures on the torsional fatigue strength of an alloy steel, *Proc. Int. Conf. Fatigue Met.* (1956) 138–149.
- [28] K. Dang Van, Macro-micro approach in high-cycle multiaxial fatigue, *Adv. Multiaxial Fatigue*, ASTM STP

1191. 1191 (1993) pp. 120–130.
- [29] D.L. McDiarmid, A general criterion for high cycle multiaxial fatigue failure, *Fatigue Fract. Eng. Mater. Struct.* 14 (1991) 429–453.
- [30] K.N. Smith, P. Watson, T.H. Topper, A stress-strain function for the fatigue of metals, *J. Mater.* 5 (1970) 767–778.
- [31] S. Fouvry, K. Elleuch, G. Simeon, Prediction of crack nucleation under partial slip fretting conditions, *J. Strain Anal. ImechE.* 37 (2002) 549–564.